Electron momentum distribution of decagonal $Al_{72}Ni_{12}Co_{16}$ studied by Compton scattering

2002 J. Phys.: Condens. Matter 14 L43

(http://iopscience.iop.org/0953-8984/14/2/102)

INSTITUTE OF PHYSICS PUBLISHING JOURNAL OF PHYSICS: CONDENSED MATTER

J. Phys.: Condens. Matter **14** (2002) L43–L48 PII: S0953-8984(02)28788-3

LETTER TO THE EDITOR

Electron momentum distribution of decagonal $Al_{72}Ni_{12}Co_{16}$ studied by Compton scattering

Junpei Tamura Okada[1], Yasuhiro Watanabe[1], Yoshihiko Yokoyama[2], Nozomu Hiraoka[3], Masayoshi Itou[3], Yoshiharu Sakurai[3] and Susumu Nanao[1]

[1] Institute of Industrial Science, University of Tokyo, 4-6-1 Komaba, Meguro, Tokyo 153-8505, Japan
[2] Himeji Institute of Technology, 2167 Shosha, Himeji 671-2201, Japan
[3] Japan Synchrotron Radiation Research Institute (JASRI), SPring-8, 1-1-1 Kouto, Mikazuki, Sayo, Hyogo 679-5198, Japan

Received 5 September 2001, in final form 23 November 2001
Published 13 December 2001
Online at stacks.iop.org/JPhysCM/14/L43

Abstract

The electron-momentum-density distributions (Compton profiles) in decagonal $Al_{72}Ni_{12}Co_{16}$ have been measured along the [00002] and [11000] directions with a momentum resolution of 0.14 au. The experimental valence-electron profile is decomposed into two partial profiles: an inverted parabola-like profile and a broad Gaussian-like profile. By fitting the broad partial profile with a profile made up of atomic 3d wavefunctions, it is found that a considerable portion of the 3d-electron holes of Ni and Co are filled with electrons. The directionally averaged radius of the Fermi sphere is estimated from the number of electrons under the parabolic partial profile. The radius is larger than that of the inscribed sphere of the quasi-Brillouin zone. This leads to the Hume-Rothery mechanism does not play an important role in explaining the stability of the decagonal quasicrystal. Slight anisotropies of the Compton profile are observed.

Quasicrystals (QCs) are metallic alloys that possess a long-range structural order, while their rotational symmetries are incompatible with the long-range periodicity in the crystals. The unusual structural properties of the alloys accompany physical properties unexpected in conventional metallic alloys. While the local atomic structures as well as the geometrical frameworks of the QCs have been made clear using x-ray and neutron diffraction and high-resolution electron microscopy, the properties of the valence electrons still remain largely unaccounted for. One of the issues is the geometrical relation between the Fermi surface (FS) and the quasi-Brillouin zone (q-BZ) that is defined by dominant Bragg diffraction spots. This knowledge is indispensable to examination of possible explanations for the stability and the anomalous transport properties of the QCs. If the FS is fairy well defined, and its size and the size of the inscribed sphere of the q-BZ are very close, the interaction between them

will produce a pseudogap of a few hundreds of meV at the Fermi level (E_F) [1, 2], possibly lowering the electronic energy to stabilize the QCs and enhancing the electrical resistivity [3]. In the case of icosahedral QCs (i-QCs), the q-BZ is an icosahedral polyhedron which is very close to a sphere. When the FS touches the q-BZ boundary at many places, the total energy of the valence electrons is effectively reduced due to the Hume-Rothery mechanism [4]. Tanaka *et al* [5] have carried out measurements of high-resolution Compton profiles of Al–Li–Cu i-QCs and have shown that the nearly spherical FS touches the q-BZ boundary, supporting the Hume-Rothery mechanism in the Al–Li–Cu i-QCs.

Unlike the i-QCs, decagonal QCs (d-QCs) possess a periodic crystalline order along the tenfold axis and a quasiperiodic order in the planes normal to the axis. The electronic properties of d-QCs have been studied by means of electrical resistivity, Hall effect, thermoelectric power, and thermal and optical conductivity measurements [4]. All of the results display strong anisotropic properties; i.e., metallic behaviour is found along the periodic direction while nonmetallic behaviour appears in the planes with the quasiperiodic order. Theoretically, Trambly de Laissardière and Fujiwara [6] have investigated a model approximant, $Al_{66}Cu_{20}Co_{14}$, of the Al–Cu–Co d-QC by a self-consistent, linear-muffin-tin-orbital method in an atomic sphere approximation, and have predicted a broad pseudogap to appear at E_F in the same way as in the i-QCs. Sabiryanov and Bose [7] and Sabiryanov *et al* [8] have made calculations for higher-order model approximants, and have demonstrated that the existence of the pseudogap depends on both the chemical composition and the local structure around the transition metal atoms. Krajčí *et al* [9] have performed systematic studies on the decagonal, icosahedral, and crystalline phases in the Al–Pd–Mn system, and have concluded that the pseudogap opening does not necessarily account for the stability of d-QCs. Experimentally, photoemission experiments on $Al_{70}Ni_{15}Co_{15}$ d-QCs [10] have not displayed any pseudogap structures at E_F. However, high-resolution ultraviolet photoemission spectroscopy of $Al_{70}Ni_{15}Co_{15}$ d-QCs [2] and electron energy-loss spectroscopy of $Al_{70}Ni_{15}Co_{15}$ d-QCs [11] have revealed fine structures near E_F. Until now, the theoretical investigations and the spectroscopic experiments have provided contradictory results on the existence of the pseudogap which arises from the FS—q-BZ interaction in the Hume-Rothery scenario.

In this work, high-resolution Compton profiles of decagonal $Al_{72}Ni_{12}Co_{16}$ (d-AlNiCo) have been measured. By analysing the profiles, we present the geometrical relation between the experimentally determined FS and the q-BZ, to provide a new observation supporting the validity of the Hume-Rothery mechanism in d-AlNiCo.

It is well known that in a Compton scattering experiment one obtains the so-called Compton profile $J(p_z)$ [12]:

$$J(p_z) = \iint n(\boldsymbol{p})\,\mathrm{d}p_x\,\mathrm{d}p_y \tag{1}$$

where $n(\boldsymbol{p})$ is the ground-state electron momentum density. In the independent-particle model,

$$n(\boldsymbol{p}) = \sum_i |\psi_i(\boldsymbol{r})\exp(\mathrm{i}\boldsymbol{p}\cdot\boldsymbol{r})\,\mathrm{d}\boldsymbol{r}|^2 \tag{2}$$

where $\psi_i(\boldsymbol{r})$ is an electron wavefunction. The summation in (2) extends over all the occupied states. The area under the Compton profile gives the total number of electrons N:

$$\int_{-\infty}^{+\infty} J(p_z)\,\mathrm{d}p_z = N. \tag{3}$$

When the profile can be decomposed into a few partial profiles each of which has a characteristic shape of a specific electronic state, then the area under a partial profile gives the number of electrons in that state.

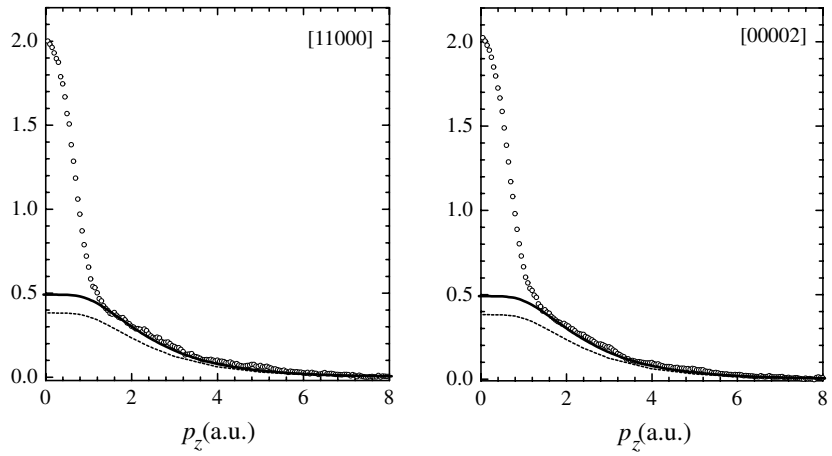

Figure 1. Experimental valence-electron Compton profiles of decagonal $Al_{72}Ni_{12}Co_{16}$ (open circles). The dashed curve represents the nominal d-electron profile which is given by the concentration-weighted sum of the Ni($3d^8$) and Co($3d^7$) free-atom profiles. The thick full curve represents the fitted d-electron profile (see the text).

A single grain of decagonal $Al_{72}Ni_{12}Co_{16}$ alloy was grown by a Czochralski method [13]. The specimen was a cylinder 35 mm in diameter and 63 mm in height. The Compton profile measurements were carried out at the BL08W, SPring-8 [14]. The energy of the incident x-rays was 116 keV and the scattering angle was 165°. For details of the spectrometer, we refer the reader to Hiraoka *et al* [15]. The energy spectra of Compton-scattered x-rays were measured along the [00002] and [11000] directions, where the index defined by Yamamoto and Ishihara [16] is used. The overall experimental momentum resolution was 0.14 au. The data processing to deduce the Compton profiles from the raw energy spectra consists of the following procedures: background subtraction; and energy-dependent corrections for the Compton scattering cross-section, the absorption of incident and scattered x-rays in the sample, the efficiency of the analyser and the detector, and the multiple scattering. Subtracting the theoretical core-electron profile $J_c(p_z)$, the valence-electron Compton profile $J_v(p_z)$ is obtained. Here, $J_c(p_z)$ is obtained from the theoretical data based on the free-atom Hartree–Fock calculation by Biggs *et al* [17], where $(1s)^2(2s)^2(2p)^6$ for Al and $(1s)^2(2s)^2(2p)^6(3s)^2(3p)^6$ for Ni and Co are treated as the core electrons.

The valence-electron Compton profiles ($J_v(p_z)$) obtained are shown in figure 1. The experimental $J_v(p_z)$ consists of two distinct parts: one is an inverted parabola with a tail of some intensity in the region of $|p_z| < 1.5$ au and the other is a broad Gaussian-like profile extended to $|p_z|$ above 5.0 au. Since the broad profile is very similar to the profile of filled d bands observed in pure metals, first we assumed that the broad partial profile was given by a profile composed as the nominal concentration-weighted sum of the profiles of Ni($3d^8$) and Co($3d^7$) free atoms [17]. We call this the nominal d-electron profile. However, as shown by the dashed curve in figure 1, the nominal d-electron profile is too low to explain the broad part of the experimental profile. Then, we assumed that the actual average number of d electrons per transition metal atom is larger than the nominal value of 7.43. By multiplying the nominal d-electron profile by a single parameter, we tried to fit it to the broad partial profile in the range between $p_z = 6$ and 8 au. The best fit was obtained with a multiplier of 1.29. The fitted d-electron profiles are shown in figure 1 by thick full curves. The area under the fitted d-electron profile gives 9.58 electrons. This value suggests that a considerable number of s, p

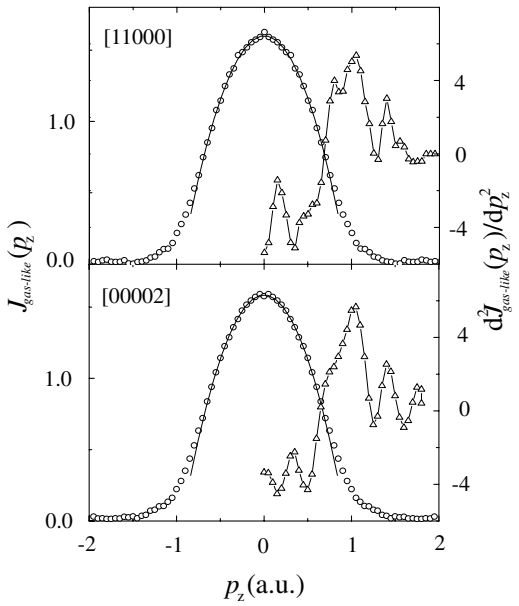

Figure 2. Profiles of the parabolic part along the [11000] and [00002] directions (open circles). The solid curves are the inverted parabolas fitted in the range between −0.6 and +0.6 au. The open triangles show the second derivatives of the profiles.

electrons are transferred into the 3d-electron states. Although the analysis is based on a crude atomic model, the result implies that the d holes of Ni and Co are nearly filled with electrons.

By subtraction of the 3d-electron part from $J_v(p_z)$, we get the partial profile of the inverted parabola with a tail (see figure 2). The resultant part, $J_{\text{gas-like}}(p_z)$, is well fitted with an inverted parabola in the range from $p_z = -0.6$ to +0.6 au, implying that an electron gas model can be employed as a basis for further discussions on the electron system of this part. For momenta higher than $|p_z| = 0.6$ au, however, a significant deviation from the parabola is observed. The deviation from the inverted parabola arises from the electron–electron and the electron–lattice interactions.

Qualitative considerations of the momentum density of an electron gas and its Compton profile are reported by Eisenberger *et al* [18]. The electron momentum density of a free (noninteracting) electron gas is the Fermi–Dirac distribution, which gives a Compton profile that is a characteristic inverted parabola with a cut-off at the Fermi momentum p_F. When the electron–electron interactions are turned on (homogeneously interacting electron gas), a tail appears beyond p_F, yielding a Compton profile that is nearly an inverted parabola in shape, but with a smeared cut-off at the same p_F and a tail at higher momenta. Further, when the homogeneously interacting electron gas is immersed into a lattice of ions (inhomogeneously interacting electron gas), as in the case of real metals, the electron–lattice interactions make the Fermi sphere anisotropic and cause additional high-momentum components centred at reciprocal-lattice points $\boldsymbol{G}$ due to the Umklapp processes. Therefore, anisotropy appears in the Compton profile. However, the observed valence-electron profiles of Li [19] and Al [20] have shown that the main part of the profiles is still very close to an inverted parabola and the anisotropies are small. In these cases the area under each Compton profile remains the same. Thus, when the anisotropy in the profile is small, to a good approximation the directionally averaged p_F can be derived from the area under the profile. In figure 2, the areas under $J_{\text{gas-like}}(p_z)$ between $p_z = -3.5$ and +3.5 au give 2.08 ± 0.11 electrons for the [11000]

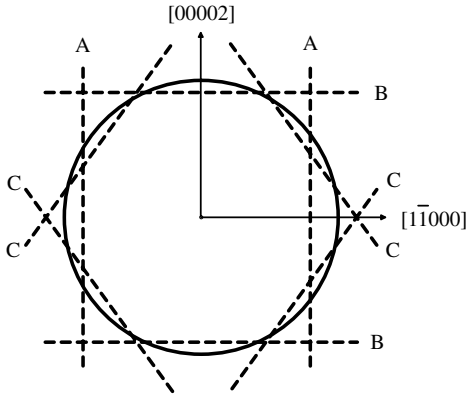

Figure 3. A schematic drawing of the (11000) cross-section of the q-BZ, together with the Fermi sphere with a radius of 0.86 au. The lines A, B, and C represent the quasi-Brillouin zone boundaries made of (23200), (00002), and (23201) Bragg diffraction planes, respectively (see table 1).

Table 1. The multiplicity and intensity of the dominant Bragg diffraction planes [21], and the radius of the inscribed sphere of the q-BZ corresponding to the Bragg diffraction planes.

Index	Multiplicity	Intensity of Bragg diffraction	Radius of inscribed sphere (au)	Line
23200	10	3	0.710	A
00002	2	40	0.814	B
23201	20	5	0.819	C

direction and 2.13 ± 0.09 electrons for the [00002] direction. The momentum range was determined so as to cover the high-momentum components at $\boldsymbol{G} = \langle 23200 \rangle$, $\langle 00002 \rangle$, and $\langle 23201 \rangle$. From this, the directionally averaged p_F is calculated to be 0.86 ± 0.01 au using the relation between p_F and the number of electrons n: $p_F = (3\pi^2 n)^{1/3}$.

Another way to estimate p_F is to find the position of a peak in the second-derivative curve of $J_{\text{gas-like}}(p_z)$ [19]. The experimental second derivatives for both directions (see figure 2) exhibit a peak around $p_z = 1.0$ au, which is slightly larger than the value obtained from the area under the profile. This difference comes from the high-momentum tail beyond p_F and the high-momentum components appearing in the Compton profiles due to the electron–electron and electron–lattice interactions. These considerations lead to the conclusion that the directionally averaged p_F of d-AlNiCo is between 0.86 and 1.0 au.

A schematic drawing of the (11000) cross-section of the q-BZ that is defined by the observed strong Bragg diffraction spots is shown in figure 3, together with the Fermi sphere with a radius of 0.86 au. The lines A, B, and C give the dominant q-BZ boundaries corresponding to the (23200), (00002), and (23201) Bragg diffraction planes (see table 1). It is clear that the Fermi sphere is larger than the q-BZ, and hence this indicates that the Hume-Rothery mechanism does not play an important role in explaining the stability of the decagonal QCs.

Slight anisotropies ($J_{00002}(p_z) - J_{11000}(p_z)$) are observed, as shown in figure 4. Since the maximum anisotropy is only about 1% of $J_v(p_z = 0)$ and just above the statistical accuracy, it may only be said, on the basis of the scenario of the electron gas immersed in the lattice, that the anisotropy is probably caused by slightly larger high-momentum components along the [00002] direction. Since the (00002) Bragg diffraction is the strongest present (table 1), it is reasonable to suppose that there are larger high-momentum components in this direction.

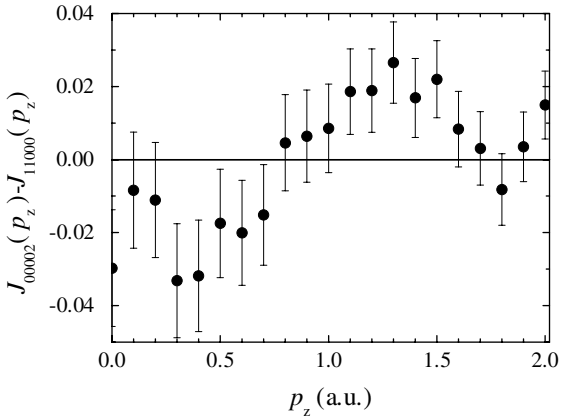

Figure 4. The Compton profile anisotropy between the [00002] and [11000] directions.

We are grateful to Professor Shiotani and Professor Kimura for illuminating discussions. The Compton profile measurements were performed with the approval of JASRI (Proposal No 2000A0246-ND-np). This work was supported in part by a Grant-in-Aid from the Ministry of Education, Culture, Sports, Science and Technology of Japan and the Light Metal Educational Foundation, Incorporated. It was also supported by the SPring-8 Research Promotion Scheme under the auspices of the Japan Science and Technology Corporation.

References

[1] Belin E, Dankhazi Z, Sadoc A, Dubois J M and Calvayrac Y 1994 *Europhys. Lett.* **26** 677
[2] Stadnik Z M, Purdie D, Garnier M, Baer Y, Tsai A P, Inoue A, Edagawa K, Takeuchi S and Buschow K H J 1997 *Phys. Rev.* B **55** 10 938
[3] Smith A P and Ashcroft N W 1987 *Phys. Rev. Lett.* **59** 1365
[4] Stadnik Z 1999 *Physical Properties of Quasicrystals (Springer Series in Solid-State Sciences vol 126)* (Berlin: Springer)
[5] Tanaka Y, Sakurai Y, Nanao S, Shiotani N, Ito M, Sakai N, Kawata H and Iwazumi T 1994 *J. Phys. Soc. Japan* **63** 3349
[6] Trambly de Laissardière G and Fujiwara T 1994 *Phys. Rev.* B **50** 9843
[7] Sabiryanov R F and Bose S K 1994 *J. Phys.: Condens. Matter* **6** 6197
[8] Sabiryanov R F, Bose S K and Burkov S E 1995 *J. Phys.: Condens. Matter* **7** 5437
[9] Krajčí M, Hafner J and Mihalkovič M 1996 *Europhys. Lett.* **34** 207
[10] Stadnik Z M, Zhang G W, Tsai A P and Inoue A 1995 *Phys. Rev.* B **51** 11 358
[11] Terauchi M, Ueda H, Tanaka M, Tsai A P, Inoue A and Masumoto T 1998 *Phil. Mag. Lett.* **77** 351
[12] Cooper M J 1985 *Rep. Prog. Phys.* **48** 415
[13] Yokoyama Y, Note R, Kimura S, Inoue A, Fukaura K and Sunda H 1997 *Mater. Trans. JIM* **38** 943
[14] Sakurai Y 1998 *J. Synchrotron Radiat.* **5** 208
[15] Hiraoka N, Itou M, Ohata T, Mizumaki M, Sakurai Y and Sakai N 2001 *J. Synchrotron Radiat.* **8** 26
[16] Yamamoto A and Ishihara K N 1988 *Acta Crystallogr.* A **44** 707
[17] Biggs F, Mendelsohn L B and Mann J B 1975 *At. Data Nucl. Data Tables* **16** 201
[18] Eisenberger P, Lam L, Platzman P M and Schmidt P 1972 *Phys. Rev.* B **10** 3671
[19] Sakurai Y, Tanaka Y, Bansil A, Kaprzyk S, Stewart A T, Nagashima Y, Hyodo T, Nanao S, Kawata H and Shiotani N 1995 *Phys. Rev. Lett.* **74** 2252
[20] Ohata T, Itou M, Matsumoto I, Sakurai Y, Kawata H, Shiotani N, Kaprzyk S, Mijnarends P E and Bansil A 2000 *Phys. Rev.* B **62** 16 528
[21] Kek S and Mayer J 1993 *Z. Kristallogr.* **205** 235